

## Molecular Magnetism

International Edition: DOI: 10.1002/anie.201804075  
German Edition: DOI: 10.1002/ange.201804075

## Magnetic Properties of a Terbium–[1]Ferrocenophane Complex: Analogies between Lanthanide–Ferrocenophane and Lanthanide–Bisphthalocyanine Complexes

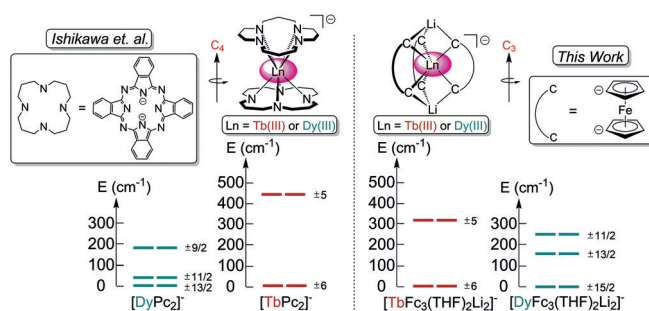
Trevor P. Latendresse, Veacheslav Vieru, Branford O. Wilkins, Nattamai S. Bhuvanesh, Liviu F. Chibotaru,\* and Michael Nippe\*

**Abstract:** A rare example of an organometallic terbium single-ion magnet is reported. A  $Tb^{3+}$ –[1]ferrocenophane complex displays a larger barrier to magnetization reversal than its isostructural  $Dy^{3+}$  analogue, which is reminiscent of trends observed for lanthanide–bis-phthalocyanine complexes. Detailed *ab initio* calculations support the experimental observations and suggest a significantly larger ground-state stabilization for the non-Kramers ion  $Tb^{3+}$  in the Tb complex than for the Kramers-ion  $Dy^{3+}$  in the Dy complex.

The unique electronic structure of the lanthanide ions engenders intriguing magnetic and photophysical properties. Molecular lanthanide complexes are finding widespread interest in areas ranging from catalysis to luminescence-based sensing and molecular information storage and processing.<sup>[1–3]</sup> The large magnetic single-ion anisotropy of trivalent lanthanide ions, such as  $Dy^{3+}$ ,  $Tb^{3+}$ , and  $Er^{3+}$ , can be exploited to furnish molecules that display slow magnetic relaxation as well as magnetic hysteresis that are of purely molecular origin.<sup>[4]</sup> The realization of molecule-sized magnetic memory can lead to progress towards new spintronic devices and high-density data storage.<sup>[3]</sup> Molecules that display such magnetic properties as a function of a single spin-carrying ion are therefore termed single-ion magnets (SIMs).<sup>[5]</sup> In 2003, Ishikawa et al. reported the first SIM,  $[TbPc_2]^-$  ( $Pc^{2-}$  = phthalocyanine), in which the square antiprismatic geometry of the axial  $Pc^{2-}$  ligands strongly stabilizes the magnetic  $m_J = \pm 6$  ground state, resulting in an effective magnetization reorientation energy barrier ( $U_{eff}$ ) of  $230\text{ cm}^{-1}$  in the absence of an external magnetic field for the magnetically dilute species.<sup>[6]</sup> Beyond the development of  $[TbPc_2]^-$  chemistry,<sup>[7]</sup> only a few new classes of  $Tb^{3+}$  SIM systems have

been reported which typically display  $U_{eff}$  values of less than  $100\text{ cm}^{-1}$ .<sup>[8]</sup> On the other hand, increased attention has been given to  $Dy^{3+}$  complexes which resulted in recent discoveries of record barriers and blocking temperatures.<sup>[9]</sup>

Recently, our group reported the first Ln–[1]ferrocenophane complex  $[Li(THF)_4][DyFc_3(THF)_2Li_2]$  (**2**), which functions as a SIM ( $U = 110\text{ cm}^{-1}$ ).<sup>[10]</sup> The molecular structure of **2**, features three diferrocenyl ligand moieties surrounding a central  $Dy^{3+}$  ion in a distorted trigonal prismatic geometry, as defined by an average twist angle lying between  $9^\circ$  and  $12^\circ$ . We hypothesized that compounds such as **2**, could be considered approximate threefold symmetric analogues of the  $D_{4d}$  sandwich-type geometry of the iconic  $[Ln(Pc)_2]^-$  series (Scheme 1). Importantly,  $[Dy(Pc)_2]^-$  complexes display smaller  $U_{eff}$  values than  $[Tb(Pc)_2]^-$  complexes.<sup>[6]</sup> We therefore



**Scheme 1.** Comparison of low-lying energy levels of  $[Ln(Pc)_2]^-$  (acquired from Ref. [6]) and  $[Ln(Fc)_3Li_2]^-$  complexes.

envisioned that the unique  $Fc_3^{6-}$  ligand architecture in systems like **2** could promote ground state bistability and improved magnetization dynamics in complexes of the non-Kramers ion  $Tb^{3+}$ . Herein, we report the synthesis, structural characterization, and magnetism of  $[Li(THF)_4][TbFc_3(THF)_2Li_2]$  (**1**), which is the first Ln–[1]ferrocenophane SIM utilizing a non-Kramers ion as the magnetic anisotropy center. Furthermore, we provide further insight into the origin of the magnetic anisotropy and magnetization dynamics of **1** and **2** using multi-configuration *ab initio* computational methods.

The preparation of **1** proceeds analogously to the previously reported  $Dy^{3+}$  congener (Supporting Information, Scheme S1).<sup>[10]</sup> Addition of anhydrous  $TbX_3$  ( $X = Cl^-$  or  $I^-$ ) to a solution containing 1.33 equiv of  $Li_6Fc_3(TMEDA)_2$  in THF results in a slightly cloudy red/brown solution, which is subsequently filtered. Upon removal of the solvent and

[\*] T. P. Latendresse, B. O. Wilkins, Dr. N. S. Bhuvanesh, Prof. Dr. M. Nippe  
Department of Chemistry, Texas A&M University  
3255 TAMU, College Station, TX 77843 (USA)  
E-mail: nippe@tamu.edu

Dr. V. Vieru, Prof. Dr. L. F. Chibotaru  
Theory of Nanomaterials Group, Katholieke Universiteit Leuven  
Celestijnenlaan 200F, 3001 Leuven (Belgium)  
E-mail: Liviu.Chibotaru@chem.kuleuven.be

Supporting information (including experimental and computational details, including synthetic protocol, crystallography information, structure tables, and magnetic characterization methods) and the ORCID identification number(s) for the author(s) of this article can be found under:  
<https://doi.org/10.1002/anie.201804075>.

extraction of the crude product into diethyl ether, large pyrophoric orange crystals of pure **1** are readily obtained in yields between 17–23% by recrystallizing of the crude product from THF/pentane mixtures at  $-27^{\circ}\text{C}$ .

Single-crystal X-ray diffraction established that compound **1** is isostructural to **2** (Figure 1; Supporting Information, Tables S1, S2). Compound **1** crystallizes in the space group  $P2_1/c$  and contains two anionic  $[\text{Tb}(\text{Fc})_3(\text{THF})_2\text{Li}_2]^-$  molecules per asymmetric unit, **Tb(1)** and **Tb(2)**. Each

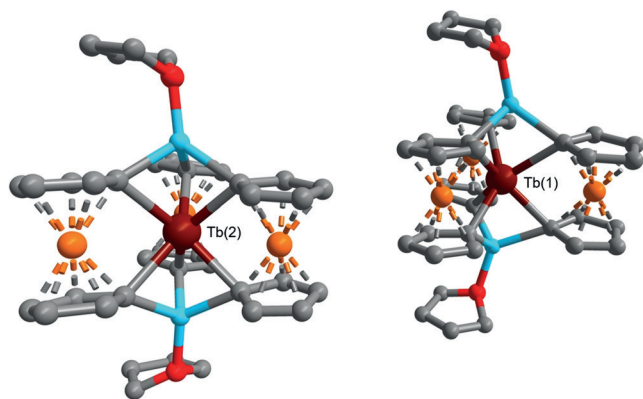


**Figure 1.** Molecular structures of the two crystallographic independent monoanionic  $[\text{TbFc}_3(\text{THF})_2\text{Li}_2]^-$  molecules in **1**. Hydrogen atoms and counter cations have been omitted for clarity. Tb maroon, Fe orange, O red, C gray, Li light blue.<sup>[23]</sup>

molecule of **1** features a six-coordinate distorted trigonal prismatic crystal-field geometry in which three diferrocenyl moieties chelate the central  $\text{Tb}^{3+}$  ion (see the Supporting Information, Table S5 for parameters calculated using the SHAPE program<sup>[11]</sup>). It should be noted, however, that even for a structure close to ideal geometry, the crystal-field parameters for lanthanides can deviate strongly from the predicted ones for ideal geometries<sup>[12]</sup> (Supporting Information, Table S15). The anionic charge of each molecule is balanced by three  $\text{Li}^+$  ions, where two  $\text{Li}^+$  ions are found to reside in the inner coordination sphere inside an anionic pocket formed by the diferrocenyl C1 ligand donors and the third as an outer-sphere  $[\text{Li}(\text{THF})_4]^+$  cationic unit. The average Tb–C bond distances of 2.56[2] Å (**Tb(1)**) and 2.55[2] Å (**Tb(2)**) are within statistical error similar to the corresponding distances found in **2** (2.547[5] Å and 2.544[5] Å). The same trend holds for the average Tb– $\text{Fe}_{\text{avg}}$  interatomic distances ranging from 3.193(4)–3.269(4) Å ( $\text{Dy–Fe}_{\text{avg}}$ : 3.185(4)–3.262(4) Å for **2**). The average twist angle of **1** between 8–10° suggests the crystal field is slightly closer to ideal trigonal prismatic geometry than in compound **2** (the average twist angle for **2** is 9–12°). The higher symmetry in **1** is likely due to the larger ionic radius of  $\text{Tb}^{3+}$ , which decreases the steric hindrance of the diferrocenyl ligands.

The static magnetic properties of **1** were investigated by direct current (dc) magnetometry. The temperature dependence of the molar magnetic susceptibility temperature product ( $\chi_M T$ ) of restrained, randomly oriented crystallites of **1** under a 500 Oe external magnetic field between 300 K and 2 K is shown in Figure S1. The  $\chi_M T$  (300 K) value of

11.96  $\text{emu K mol}^{-1}$  is close to the expected value of 11.82  $\text{emu K mol}^{-1}$ , which confirms the presence of a single  $\text{Tb}^{3+}$  ion ( ${}^7\text{F}_6$ ,  $S=3$ ,  $L=3$ ,  $g=3/2$ ) and the diamagnetic nature of the ligand moieties (low-spin  $\text{Fe}^{2+}$ ;  $S=0$ ). Upon cooling, the  $\chi_M T$  value remains nearly constant, decreasing only slightly between 300 K and 5 K. At 5 K, a steeper decrease in the  $\chi_M T$  value is observed to a minimum value of 10.68  $\text{emu K mol}^{-1}$  at 2 K. For mononuclear  $\text{Ln}^{3+}$  complexes, the low-temperature deviation of the magnetic susceptibility from predicted Curie Law behavior can be attributed to molecular magnetic anisotropy, depopulation of the magnetic excited states, and/or blocking of the magnetization. To further investigate the intrinsic magnetic anisotropy and crystal field effects of **1**, the magnetization was measured up to 7 T in the temperature range of 8 K to 2 K. At 2 K, the magnetization approaches saturation around 4 T at a value of 4.78  $\mu_B$  and increases only slightly to a value of 4.85  $\mu_B$  at the instrument field limit of 7 T (Supporting Information, Figure S2). The deviation of  $M_S$  from the expected value of 9.0  $\mu_B$  suggests the crystal field has split the  ${}^7\text{F}_6$  electronic state into individual  $m_j$  states. The non-superposition of the  $M$  vs.  $H/T$  curves at each temperature suggests significant magnetic anisotropy is present in **1** (Supporting Information, Figure S3).

The dynamic magnetic properties of **1** were initially investigated using alternating current (ac) magnetometry between 1–1000 Hz in the absence of an applied dc magnetic field. A single temperature-dependent signal (see below) is observed in the out-of-phase component of the molar ac susceptibility ( $\chi_M''$ ) vs. frequency plot of **1** between 2 K and 28 K (Figure 2 top; for in-phase component ( $\chi_M'$ ) see the Supporting Information, Figure S4). Between 2 K and 6 K, the  $\chi_M''$  signal of **1** remains largely temperature independent which is similar to what has been observed for compound **2**. At temperatures above 8 K, the  $\chi_M''$  maximum becomes increasingly temperature dependent, likely due to a transitioning of the relaxation into an Orbach mechanism at 20 K which is also further supported by the linear region in the Arrhenius plots of **1** (see below). The temperature-independent nature of the  $\chi_M''$  maximum at low temperatures is commonly observed in many SIMs and is an indication of QTM, which describes spin reorientation that proceeds through a non-classical, thermally unassisted, pathway. Quantum tunneling relaxation can be promoted by intermolecular dipole–dipole interactions between neighboring spin centers within the crystal lattice, which causes resonance of the wave functions of magnetic states with opposing orientation.<sup>[13]</sup> To mitigate potential dipole–dipole interactions between neighboring molecules, compound **1** was co-crystallized with the isostructural diamagnetic analogue  $[\text{Li}(\text{THF})_4][\text{YFc}_3(\text{THF})_2\text{Li}_2]$  (**3**), in a 1:12.2 Tb:Y ratio (**1-dilute**). The fully temperature-dependent nature of the  $\chi_M''$  signal over the 16–34 K temperature range (Figure 2 middle, for  $\chi_M'$  see the Supporting Information, Figure S6) suggests that dilution of **1** indeed lowers QTM probability caused by intermolecular dipole–dipole interactions, which are important to the spin relaxation of **1** under zero dc field at low temperatures. An alternate method for decreasing QTM processes is the application of external dc field bias, which effectively breaks

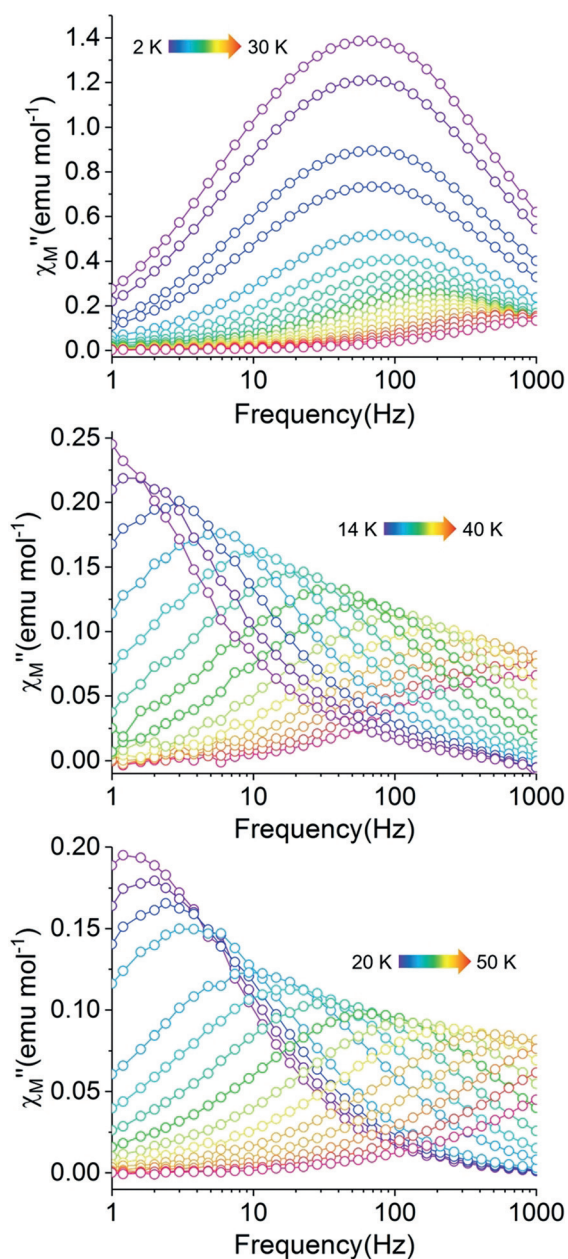


**Figure 2.** Plots of the temperature dependence of the out-of-phase component of the molar ac susceptibility ( $\chi_M''$ ) versus frequency of **1** where  $H_{dc} = 0$  Oe (top), **1-dilute** where  $H_{dc} = 0$  Oe (middle), and **1** where  $H_{dc} = 4800$  Oe (bottom).

the degeneracy of the  $\pm m_J$  magnetic states and decreases QTM transition probabilities. The field dependence of the ac susceptibility of concentrated samples of **1** at 28 K is shown in the Supporting Information, Figures S8, S9. The field dependence of the magnetic relaxation time ( $\tau$ ) (Supporting Information, Figure S11; extracted from Cole–Cole plots (Supporting Information, Figure S10) by using the general Debye equation, see below) displays the expected increase in  $\tau$  with increasing fields. However, a commonly observed decrease of  $\tau$  at large fields (owing to increased contributions to field induced direct relaxation processes) is not observed in the case of **1** up to applied field strengths of 0.72 T. Similar field

dependence of  $\tau$  has been observed in a mononuclear transition metal SIMs.<sup>[14]</sup> We therefore decided to acquire variable temperature ac susceptibility data using an applied field of 4800 Oe, which does decrease the participation of QTM processes and minimizes effects from field-induced direct processes. As shown in Figure 2 (bottom), the  $\chi_M''$  maximum of **1@4800** becomes fully temperature dependent and remains within the ac frequency range up to temperatures of 46 K.

The spin relaxation times ( $\tau$ ) and the relaxation time distribution parameters ( $\alpha$ ) of **1**, **1-dilute**, **1@4800** were determined at each temperature by fitting the Cole–Cole curves ( $\chi_M''$  vs.  $\chi_M'$ ) with the general Debye equation (Supporting Information, Figure S5, S7, S13). For **1**, the broad nature of the Cole–Cole curves across the full temperature range corresponds to a relatively wide distribution of relaxation times ( $\alpha = 0.191$ – $0.387$ ), and suggests multiple spin relaxation processes are occurring at similar ac frequencies.<sup>[15]</sup> A decrease in  $\alpha$  upon heating indicates that spin relaxation is moving towards a single, thermally activated mechanism.

The relaxation times at each temperature were used to construct Arrhenius plots ( $\ln(\tau)$  vs.  $T^{-1}$ ) for **1**, **1-dilute**, and **1@4800** (Figure 3). The lack of a horizontal region at low temperatures in the Arrhenius plots of **1-dilute** and **1@4800** indicate that QTM can indeed be minimized in **1** by separating anisotropic centers or by creating a field bias, respectively. The Arrhenius plots were fit over the whole temperature range using Equation (1), which takes into account spin relaxation through QTM, Raman, and Orbach mechanisms:  $\tau^{-1} = \tau_{\text{QTM}}^{-1} + CT^n + \tau_o^{-1} \exp(-U/k_b T)$ . Typically, terms accounting for spin relaxation via direct processes ( $AH^{mT}$ ) are included in Arrhenius fits involving ac susceptibility data collected under applied dc fields. However, as discussed above, a decrease in  $\tau$  was not observed within the investigated dc field range (up to 0.72 T) and it is therefore assumed that relaxation via field induced direct processes is negligible for **1@4800**. For **1-dilute**, contributions from QTM relaxation were not included into the fitting routine. Furthermore, to avoid over-parameterization, the anisotropy barrier obtained for **1-dilute** was held constant in the fitting of

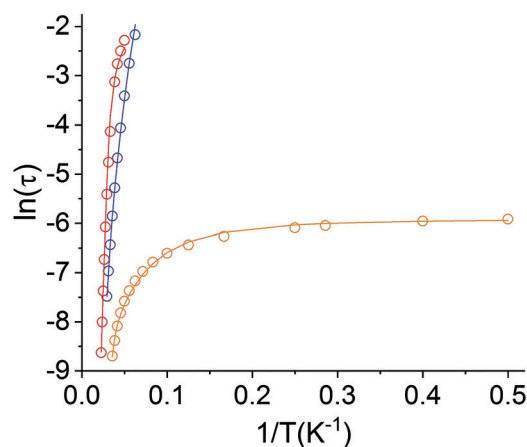


**Figure 3.** Arrhenius plots of the magnetic relaxation time of **1** (orange), **1-dilute** (blue), and **1@4800** (red). Solid lines represent the line of best fit of the thermally activated temperature regime.

**1.** This fitting procedure yielded barriers to magnetization reversal of  $U = 274 \text{ cm}^{-1}$  ( $\tau_{\text{QTM}} = 2.69 \times 10^{-3} \text{ s}$ ,  $C = 1.99 \text{ s}^{-1} \text{ K}^{-2.25}$ ,  $n = 2.25$ ,  $\tau_0 = 3.78 \times 10^{-10} \text{ s}$ ) for **1**,  $U = 274 \text{ cm}^{-1}$  ( $\tau_{\text{QTM}} = 0 \text{ s}$ ,  $C = 6.89 \times 10^{-8} \text{ s}^{-1} \text{ K}^{-6.66}$ ,  $n = 6.66$ ,  $\tau_0 = 1.33 \times 10^{-8} \text{ s}$ ) for **1-dilute**, and  $U = 401 \text{ cm}^{-1}$  ( $\tau_{\text{QTM}} = 0.125 \text{ s}$ ,  $C = 7.95 \times 10^{-7} \text{ s}^{-1} \text{ K}^{-5.09}$ ,  $n = 5.09$ ,  $\tau_0 = 3.74 \times 10^{-10} \text{ s}$ ) for **1@4800**. Alternatively, the effective barrier to magnetization reversal can be estimated by fitting solely the linear region of the Arrhenius plot according to  $\tau^{-1} = \tau_0^{-1} \exp(-U_{\text{eff}}/k_{\text{b}} T)$  (Supporting Information, Figure S14), which resulted in  $U_{\text{eff}} = 53.9 \text{ cm}^{-1}$  ( $\tau_0 = 1.13 \times 10^{-5} \text{ s}$ ) for **1**,  $U_{\text{eff}} = 169 \text{ cm}^{-1}$  ( $\tau_0 = 4.62 \times 10^{-7} \text{ s}$ ) for **1-dilute**, and  $U_{\text{eff}} = 334 \text{ cm}^{-1}$  ( $\tau_0 = 3.55 \times 10^{-9} \text{ s}$ ) for **1@4800**. The slow relaxation dynamics of **1** lead to butterfly-shaped hysteresis up to at least 3 K (Supporting Information, Figure S15). The collapse of the magnetization upon removing the applied magnetic field is indicative of quick spin relaxation through QTM pathways, which is consistent with the low-temperature out-of-phase susceptibility data of non-dilute **1** (see below) and is similar to the observed hysteresis of compound **2**. For **1-dilute** we observe somewhat larger openings in the hysteresis loops (Supporting Information, Figure S16), which supports the presence of intermolecular magnetic interactions between neighboring  $\text{Tb}^{3+}$  centers to spin relaxation of non-dilute **1** further.

The observation that  $\text{Tb}^{3+}$  compound **1** does indeed display a higher barrier to magnetization reversal than isostructural  $\text{Dy}^{3+}$  compound **2**, parallels the reported trends for bis-phthalocyanine complexes of  $\text{Tb}^{3+}$  and  $\text{Dy}^{3+}$  and supports our initial hypothesis (see above). To elucidate the origin of this behavior further, we used the Molcas 8.2 program package to perform CASSCF/SO-RASSI/SINGLE\_ANISO as well as XMS-CASPT2/SO-RASSI/SINGLE\_ANISO calculations.<sup>[16–18]</sup> on both crystallographic independent molecules of **1** and **2** (see the Supporting Information for details). The energies and corresponding  $g$ -tensors of the low-lying spin-orbital states for both  $\text{Tb}^{3+}$  sites in **1**, and of the low-lying Kramers doublets (KD) for both  $\text{Dy}^{3+}$  sites in **2** are given in the Supporting Information, Tables S7–S14. Consistent with the very similar geometries of the two crystallographic independent molecules in **1** and **2**, calculated properties for both sites are also very similar and only results obtained of one site within XMS-CASPT2 calculations will be discussed in detail (Table 1).

Table 1 shows that the stabilization of the ground state is significantly larger for **1** than for **2**, given the calculated energies of the first excited state doublets of compound **1** ( $343 \text{ cm}^{-1}$ ) and **2** ( $180 \text{ cm}^{-1}$ ). The ground state doublets of **1** and **2** correspond to almost pure  $m_j = \pm 6$  and  $\pm 15/2$  states, respectively. The high axiality of the ground doublets in **1** (small tunneling gaps) and **2** (small transversal  $g$  factors,  $g_x$ ,  $g_y$ ) explains why both compounds exhibit SMM behavior.<sup>[20]</sup> To determine the structure of the magnetization blocking barrier (Figure 4), we applied a recently proposed approach.<sup>[21]</sup> Given the small matrix elements connecting the opposite components of KDs in **2** and the small intrinsic tunneling gap in the first excited doublet in **1**, it is expected that the relaxation of magnetization would go via the third excited doublet in the former and via the second excited doublet in the latter, as it is outlined by blue arrows in

**Table 1:** Energy [ $\text{cm}^{-1}$ ] of the low-lying spin-orbital states of Tb center in **1** and the low-lying KDs of Dy center in **2** and the  $g$  factors of the corresponding three lowest doublets.

[TbFc <sub>3</sub> (THF) <sub>2</sub> Li <sub>2</sub> ] <sup>−</sup> ( <b>1</b> )		[DyFc <sub>3</sub> (THF) <sub>2</sub> Li <sub>2</sub> ] <sup>−</sup> ( <b>2</b> )	
0		0	
$2 \times 10^{-4}$		0	
343.320		179.780	
343.328		179.780	
649.433		235.613	
649.599		235.613	
857.401		334.684	
870.377		334.684	
951.240		497.438	
956.840		497.438	
974.269		701.223	
1022.634		701.223	
1025.245		895.777	
		895.777	
		1021.102	
		1021.102	
g factors of the lowest three doublets <sup>[a]</sup>			
1	$g_x$	0	$2.88 \times 10^{-5}$
	$g_y$	0	$3.41 \times 10^{-5}$
	$g_z$	18.01	19.97
2	$g_x$	0	$4.73 \times 10^{-5}$
	$g_y$	0	$1.22 \times 10^{-4}$
	$g_z$	14.53	17.20
3	$g_x$	0	$4.55 \times 10^{-3}$
	$g_y$	0	$4.82 \times 10^{-3}$
	$g_z$	11.19	14.59

[a] The transversal  $g$  factors of the Tb complexes are zero owing to the Griffith theorem.<sup>[19]</sup>

Figure 4. However, these do not match the experimentally extracted barriers at investigated temperatures. Because these temperatures are relatively high, and given the high axiality of the ground doublets (Table 1), the relaxation is of thermally activated QTM (TA-QTM) type,<sup>[22]</sup> and occurs via the doublet  $n$  having the largest value of  $P_n \Gamma_n$ , where  $P_n$  is the Boltzmann population of the doublet and  $\Gamma_n$  is the tunneling relaxation rate for the doublet  $n$ . The latter is proportional to  $\Delta_{\text{tun}}^2$ , which in the case of **1** is the square of intrinsic gap, while in the case of **2** is defined by the transversal Zeeman splitting, that is, is proportional to  $(g_x + g_y)^2$ . The Boltzmann population is proportional to  $e^{-E_n/kT}$ . Using the energies of the first and second excited doublets of **1**, 343 and  $649 \text{ cm}^{-1}$  (Table 1) and their intrinsic tunneling gaps, we obtain  $\Gamma_2/\Gamma_3 = 4519$  for  $T = 30 \text{ K}$ , which shows that the TA-QTM relaxation certainly goes through the first excited doublet.

Remarkably, the energy of the first excited doublet  $343 \text{ cm}^{-1}$  matches well the experimentally extracted barrier  $U_{\text{eff}} = 334 \text{ cm}^{-1}$  of **1@4800** extracted from the linear region of the Arrhenius plot at 30–46 K. Note that at  $T > 70 \text{ K}$ ,  $\Gamma_3/\Gamma_2 > 1$  and a higher barrier would be observed corresponding to the energy of the second excited doublet. For **2**, the same analysis gives  $\Gamma_2/\Gamma_3 = 500$  for  $T = 20 \text{ K}$ . This tells us the TA-QTM relaxation in this case will proceed via the first excited KD of  $\text{Dy}^{3+}$  ion. The discrepancy between the experimentally extracted barrier,  $U_{\text{eff}} = 110 \text{ cm}^{-1}$ , and the calculated energy of the first excited KD ( $180 \text{ cm}^{-1}$ ) is most probably explained

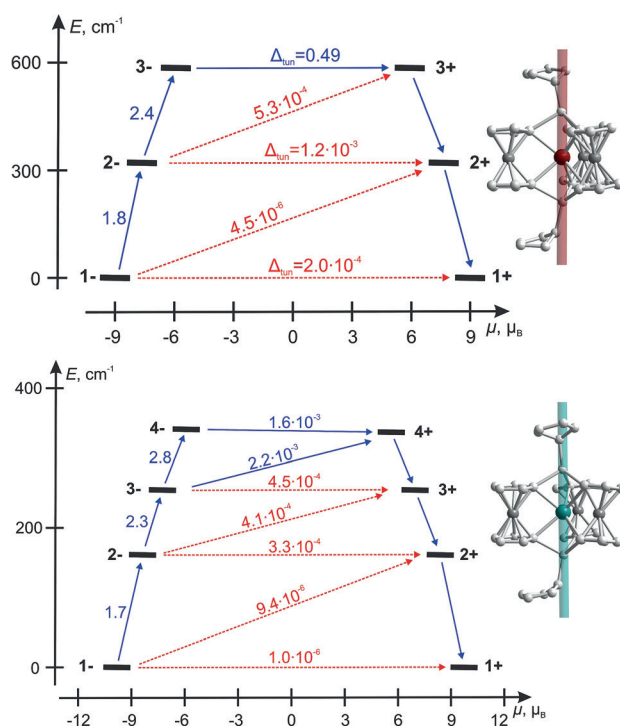


**Figure 4.** Low-lying levels and magnetization barrier in **1** (top) and **2** (bottom). Each state (horizontal thick black lines) is located according to its magnetic moment. The arrows show the transition between the states, whereas the numbers accompanying them are the average transition moments ( $\mu_B$ ) or the intrinsic tunneling gaps,  $\Delta_{\text{tun}}$  [ $\text{cm}^{-1}$ ]. The blue arrows indicate the barrier to the blocking of magnetization. The orientation of the main magnetic axes in **1** and **2** are shown by thick lines on the right side.

by the fact that the used  $\ln(\tau)$  vs.  $1/T$  curve did not reach a linear domain yet.

In conclusion, the approximate trigonal prismatic coordination environment in lanthanide-[1]ferrocenophane complexes results in a significantly larger energetic stabilization of the magnetic ground states for  $\text{Tb}^{3+}$  in **1** than for  $\text{Dy}^{3+}$  in **2**. This observation is reminiscent of previous studies on Ln-bisphthalocyanine SIMs and also suggests that future development of the new class of Ln-metallophenane complexes may lead to molecules with further improved magnetic properties.

## Acknowledgements

M.N. is grateful for financial support by The Welch Foundation (A-1880). V.V. acknowledges the postdoctoral fellowship of the Fonds Wetenschappelijk Onderzoek-Vlaanderen (FWO, Flemish Science Foundation). We thank Dr. Timothy Hughbanks for generous gift of lanthanide salt starting materials.

## Conflict of interest

The authors declare no conflict of interest.

**Keywords:** ab initio calculations · ferrocene · metallocenophane · molecular magnetism · terbium

**How to cite:** *Angew. Chem. Int. Ed.* **2018**, *57*, 8296–8169  
*Angew. Chem.* **2018**, *130*, 8296–8301

- [1] a) A. S. Dudnik, V. L. Weidner, A. Motta, M. Delferro, T. J. Marks, *Nat. Chem.* **2014**, *6*, 1100; b) D. P. Halter, C. T. Palumbo, J. W. Ziller, M. Gembicky, A. L. Rheingold, W. J. Evans, K. Meyer, *J. Am. Chem. Soc.* **2018**, *140*, 2587.
- [2] M. L. Aulsebrook, B. Graham, M. R. Grace, K. L. Tuck, *Coord. Chem. Rev.* **2017**, in Press.
- [3] a) M. Mannini, F. Pineider, P. Sainctavit, C. Danieli, E. Otero, C. Sciancalepore, A. M. Talarico, M. Arrio, A. Cornia, D. Gatteschi, R. Sessoli, *Nat. Mater.* **2009**, *8*, 194; b) M. Mannini, F. Pineider, C. Danieli, F. Totti, L. Sorace, Ph. Sainctavit, M. Arrio, E. Otero, L. Joly, J. C. Cezar, A. Cornia, R. Sessoli, *Nature* **2010**, *468*, 417; c) R. Vincent, S. Klyatskaya, M. Ruben, W. Wernsdorfer, F. Balestro, *Nature* **2012**, *488*, 357; d) M. Shiddiq, D. Komijani, Y. Duan, A. Gaita-Ariño, E. Coronado, S. Hill, *Nature* **2016**, *531*, 348; e) Y. Ding, Y. Deng, Y. Zheng, *Magnetochemistry* **2016**, *2*, 40.
- [4] a) J. D. Rinehart, J. R. Long, *Chem. Sci.* **2011**, *2*, 2078; b) D. N. Woodruff, R. E. P. Winpenny, R. A. Layfield, *Chem. Rev.* **2013**, *113*, 5110; c) Y. Chen, J. Liu, L. Ungur, J. Liu, Q. Li, L. Wang, Z. Ni, L. F. Chibotaru, X. Chen, M. Tong, *J. Am. Chem. Soc.* **2016**, *138*, 2829; d) J. Liu, Y. Chen, J. Liu, V. Vieru, L. Ungur, J. Jia, L. F. Chibotaru, Y. Lan, W. Wernsdorfer, S. Gao, X. Chen, M. Tong, *J. Am. Chem. Soc.* **2016**, *138*, 5441; e) Y. Ding, N. F. Chilton, R. E. P. Winpenny, Y. Zheng, *Angew. Chem. Int. Ed.* **2016**, *55*, 16071; *Angew. Chem.* **2016**, *128*, 16305; f) J. Lu, M. Guo, J. Tang, *Chem. Asian J.* **2017**, *12*, 2772; g) J. J. Le Roy, I. Korobkov, M. Murugesu, *Chem. Commun.* **2014**, *50*, 1602; h) K. R. Meihaus, J. R. Long, *J. Am. Chem. Soc.* **2013**, *135*, 17952; i) P. Zhang, L. Zhang, C. Wang, S. Xue, S.-Y. Lin, J. Tang, *J. Am. Chem. Soc.* **2014**, *136*, 4484.
- [5] Y. Meng, S. Jiang, B. Wang, S. Gao, *Acc. Chem. Res.* **2016**, *49*, 2381.
- [6] N. Ishikawa, M. Sugita, T. Ishikawa, S. Koshihara, Y. Kaizu, *J. Am. Chem. Soc.* **2003**, *125*, 8694.
- [7] H. Wang, B. Wang, Y. Bian, S. Gao, J. Jiang, *Coord. Chem. Rev.* **2016**, *306*, 195.
- [8] a) K. R. Meihaus, S. G. Minasian, W. W. Lukens, Jr., S. A. Kozimor, D. K. Shuh, T. Tylliszczak, J. R. Long, *J. Am. Chem. Soc.* **2014**, *136*, 6056; b) S. Demir, J. M. Zadrozny, J. R. Long, *Chem. Eur. J.* **2014**, *20*, 9524; c) X. Wang, L. Li, D. Liao, *Inorg. Chem.* **2010**, *49*, 4735; d) N. Zhou, Y. Ma, C. Wang, G. F. Xu, J. Tang, J. Xu, S. Yan, P. Cheng, L. Li, D. Liao, *Dalton Trans.* **2009**, 8489; e) E. Coronado, C. Gimenez-Saiz, A. Recuenco, A. Tarazon, F. M. Romero, A. Camon, F. Luis, *Inorg. Chem.* **2011**, *50*, 7370; f) J.-J. Wang, J. Sun, M. Yang, L.-C. Li, *Inorg. Chem.* **2015**, *54*, 11307; g) C.-X. Zhang, Z.-M. Qiao, Y.-K. Kong, B. Wang, Y.-Y. Zhang, Q.-L. Wang, *J. Mol. Struct.* **2015**, *1081*, 348; h) P. Hu, Z. Sun, X. Wang, L. Li, D. Liao, D. Luneau, *New J. Chem.* **2014**, *38*, 4716.
- [9] a) F. Guo, B. M. Day, Y. Chen, M. Tong, A. Mansikkamäki, R. A. Layfield, *Angew. Chem. Int. Ed.* **2017**, *56*, 11445; *Angew. Chem.* **2017**, *129*, 11603; b) C. A. P. Goodwin, F. Ortu, D. Reta, N. F. Chilton, D. P. Mills, *Nature* **2017**, *548*, 439.
- [10] T. P. Latendresse, N. S. Bhuvanesh, M. Nippe, *J. Am. Chem. Soc.* **2017**, *139*, 8058.
- [11] a) M. Pinsky, D. Avnir, *Inorg. Chem.* **1998**, *37*, 5575; b) D. Casanova, J. Cirera, M. Llunell, P. Alemany, D. Avnir, S. Alvarez, *J. Am. Chem. Soc.* **2004**, *126*, 1755; c) J. Cirera, E. Ruiz, S. Alvarez, *Chem. Eur. J.* **2006**, *12*, 3162.
- [12] L. Ungur, L. F. Chibotaru, *Chem. Eur. J.* **2017**, *23*, 3708.

- [13] D. Gatteschi, R. Sessoli, *Angew. Chem. Int. Ed.* **2003**, *42*, 268; *Angew. Chem.* **2003**, *115*, 278.
- [14] V. V. Novikov, A. A. Pavlov, Y. V. Nelyubina, M. Boulon, O. A. Varzatskii, Y. Z. Voloshin, R. E. P. Winpenny, *J. Am. Chem. Soc.* **2015**, *137*, 9792.
- [15] Y. Guo, G. Xu, Y. Guo, J. Tang, *Dalton Trans.* **2011**, *40*, 9953.
- [16] F. Aquilante, J. Autschbach, R. K. Carlson, L. F. Chibotaru, M. G. Delcey, L. De Vico, I. Fdez Galván, N. Ferré, L. M. Frutos, L. Gagliardi, et al., *J. Comput. Chem.* **2016**, *37*, 506.
- [17] L. F. Chibotaru, L. Ungur, *J. Chem. Phys.* **2012**, *137*, 064112.
- [18] A. A. Granovsky, *J. Chem. Phys.* **2011**, *134*, 214113.
- [19] J. S. Griffith, *Phys. Rev.* **1963**, *132*, 316.
- [20] H. L. C. Feltham, Y. Lan, F. Klöwer, L. Ungur, L. F. Chibotaru, A. K. Powell, S. Brooker, *Chem. Eur. J.* **2011**, *17*, 4362.
- [21] L. Ungur, M. Thewissen, J.-P. Costes, W. Wernsdorfer, L. F. Chibotaru, *Inorg. Chem.* **2013**, *52*, 6328.
- [22] D. A. Garanin, E. M. Chudnovsky, *Phys. Rev. B* **1997**, *56*, 11102.
- [23] CCDC 1835132 contains the supplementary crystallographic data for this paper. These data can be obtained free of charge from The Cambridge Crystallographic Data Centre.

Manuscript received: April 5, 2018

Revised manuscript received: May 4, 2018

Accepted manuscript online: May 7, 2018

Version of record online: June 6, 2018